Ceramics International 48 (2022) 18433–18440

Contents lists available at ScienceDirect

Ceramics International

journal homepage: www.elsevier.com/locate/ceramint

Structural and thermal influence of niobia in aluminoborosilicate glasses

D.L. Costa-silva [a], J.F. Bartolomé [b], A.C. Silva [a,1], S. Mello-Castanho [a,*]

[a] Instituto de Pesquisas Energéticas e Nucleares - IPEN, São Paulo, SP, 05508-900, Brazil
[b] Instituto de Ciencia de Materiales de Madrid (ICMM), Consejo Superior de Investigaciones Científicas (CSIC), Madrid, 28049, Spain

ARTICLE INFO

Keywords:
Niobium oxide
Aluminoborosilicate
Glass network structure

ABSTRACT

The addition of small amounts of niobia (Nb_2O_5) in borosilicate glasses was explored. By analysis on thermal and structural changes, we found evidences that niobium integrates the glass structure in octahedral NbO_6 coordination. Adding up to 8.0 mol% of Nb_2O_5, the oxide partially ruptured the glass structure, interfering in the BO_3/BO_4 ratio, but the predominant network configuration was maintained. Thermally, there was an increase in the processing interval and the glasses became more resistant against crystallization, with the presence of niobia. Also, the oxide contributed to a notable decrease in the viscosity of the melts. The improvement of such properties were obtained by the controlled dispersion of the oxide in the glass network structure, avoiding large areas of phase-to-phase separation to preserve the desired ability of these glasses to incorporate a wide range of elements.

1. Introduction

Borosilicate glasses exhibit a broad extent of applications, going from cookware and labware, to biomedical implants, electronic display devices and nuclear waste immobilization matrixes, due to their physical and chemical characteristics [1,2]. The interference of boron and others oxides such as aluminum in the glass structure depends on the concentration and the coordination state that these specimens take on. Boron can be three- or four-coordinated (BO_3 or BO_4), being influenced by the field strength of charge balancing cations such as Na^+ and Ca^{2+} [3–6]. Due to the open network structure, aluminoborosilicate glasses have been explored in the vitrification of galvanic wastes (GW), in which up to 40 wt% of GW containing toxic heavy metals (Cr, Ni, Cu, Zn and Pb) were stabilized in the glasses [7–10]. These transition metals and Pb (which is post-transition) can close the original spaces between the silicate tetrahedra by interconnecting them, in a function that is similar to Ca^{2+} ions [10].

To continue the exploratory studies on the activities of transition metals in these glass systems, we decided to add niobia (Nb_2O_5) to aluminoborosilicate glasses. Niobia is a versatile refractory oxide, adapting itself very easily into some glasses and glass-ceramics. Depending on the solubility of niobia in the system, the oxide can be used for different purposes such as chemical resistance and as a nucleation agent. Its behavior in the structure of phosphate glasses was investigated by Sene et al. [11] and Maeda et al. [12]. NbO_4 and NbO_6 units were detected, acting as network formers in P–O–Nb bonds, and as modifier units, that aggregate and grow as long chain structures, as the niobia content is raised, respectively. Most works found in the literature relate to additions of Nb_2O_5 to bioactive glasses, such as 45S5 Bioglass®, for bone replacement [13–16]. Nevertheless, the structural role of niobia in these systems is rather complex, and is still a matter of controversy. While Samuneva et al. [17] and Lopes et al. [18] report that niobia connects to bridging oxygens on the network structure, Francisco et al. observed phase separation in binary glasses of SiO_2–Nb_2O_5 [19]. Such behavior evidences the low chemical affinity between SiO_2 and Nb_2O_5, and contradicts the findings of references [11,12]. Also, different studies on glasses and glass-ceramics of the silicate and phosphate families have demonstrated that Nb^{5+} ions strongly tend to form liquid-liquid phases associated to alkali and alkaline earth ions, forming polyhedral structures [20–25]. The Nb dissolution through the silicate matrix is shown to be dependent on the connectivity and viscosity of the glasses. For the case of aluminoborosilicate glasses with high sodium and calcium contents, more studies are necessary to determine the influence of niobia in this glass composition on the structure and thermal properties, especially in complex systems such as borosilicates, that include B_2O_3 acting as a secondary glass former.

This work shows the results observed in the interference of small amounts of Nb_2O_5 in aluminoborosilicate glasses, and how it affects the

* Corresponding author.
E-mail address: srmello@ipen.br (S. Mello-Castanho).
[1] In memoriam.

https://doi.org/10.1016/j.ceramint.2022.03.112
Received 12 January 2022; Received in revised form 7 March 2022; Accepted 11 March 2022
Available online 16 March 2022

glass structure, and consequently the thermal properties such as processing window, viscosity and resistance to crystallization. A promising new family of niobium-modified borosilicate glasses is obtained in this study, with increased resistance to crystallization and lowered viscosity of melts, still preserving the desired ability of theses glasses to incorporate a wide range of elements in the network structure.

2. Experimental procedure

2.1. Choice criteria for the glass compositions

The parent glass composition used in this work was a borosilicate glass previously studied, in which B_2O_3 was introduced for the reduction in the melting temperature and adjusted to avoid the growth of second phases, as show the phase diagrams of this system [7–10]. Due to the strong tendency to grow niobate salts [13], new compositions were planned, replacing the main glass-forming oxide (SiO_2) with low contents of Nb_2O_5 (up to 8 mol%), in order to promote only a distortion in the glass structure, but also avoid second phases (precipitates). Therefore, the interaction of the oxide with the silicate matrix, as well as secondary glass formers and modifier oxides could be analyzed.

2.2. Glass synthesis

The glasses belonging to the system: xNb_2O_5-(44-x)SiO_2–25Na_2O-21.3CaO–7B_2O_3–2Al_2O_3-0.7K_2O were calculated in a molar base (2–8 mol%), named Gx (x = mol%), and a sample without niobia was produced for comparative purposes. Samples were prepared using reagent-grade SiO_2 (99.0 wt%; Vetec, Brazil), CaO (95.0 wt%, Vetec, Brazil), NaOH (97.0 wt%; Vetec, Brazil), Al_2O_3 (99.5 wt% Almatis, Brazil), H_3BO_3 (98.5 wt%, Casa Americana, Brazil), metallic Nb in powder (99.9 wt%, Brazil, Brazilian Metallurgy and Mining Company – CBMM) and K_2CO_3 (99.0 wt%, CAAL, Brazil). By homogenizing the raw materials in an agate mortar, batches were obtained, subsequently melted in ambient atmosphere using high-purity alumina crucibles, at 1300 °C during 1h in a vertical electrical furnace. The melts were then cast into pre-heated (430 °C) steel molds and annealed at this same temperature during 2h, for removal of thermal stress. Then, the samples were slowly cooled to room temperature. The annealing temperature was chosen according to previous studies involving the parent glass composition [7–10].

2.3. Characterization

Energy Dispersion X-ray Fluorescence Spectrometry (XRF) was used for chemical analyses (except for boron). Inductively Coupled Plasma - Optical Emission Spectrometry (ICP-OES) was conducted exclusively for determination of B_2O_3 content. The resulting weight percentages were converted to normalized molar percentages. X-ray diffractometry analyses of the glass samples were conducted in theta-2-theta from 5° to 70°, to confirm the amorphous character of the obtained glasses. Solid-State Magic-Angle Spinning Nuclear Magnetic Resonance (MAS-NMR) were performed. Room temperature measurements for ^{11}B (128.38 MHz) and ^{29}Si (79.49 MHz) were conducted, and spectra were generated after spun at 10 kHz with 120 scans, with a recycling time of 10 and 30 (s), to minimize saturation. The ^{93}Nb spectra were recorded at 9.4 T (97.8 MHz), spun at 10 kHz for 8000 scans, and the recycling time was 1s. Raman spectroscopy was conducted on bulk samples using a confocal Raman microscope, operating with green Ar^+ laser (532 nm), at 45 mW. The spectra obtained in the analyzes were deconvoluted using the Levenberg-Marquardt method with Gaussian-Voigt functions and the band assignments proposed by Manara et al. [26] and Lönartz et al. [27]. Differential thermal analyses (DTA) were used to determine the influence of niobia additions in the glass transition (T_g), crystallization and flow events during the heating of the samples. The experiments were performed in alumina crucibles with 14.4420 mg of glass powder for each sample, using N_2 atmosphere at 10 °C/min up to 900 °C. In order to evaluate the viscosity of the melts with different niobia contents, hot stage microscopy (HSM) was performed using a side view optical microscope with an image analyzer system and a heating system, in air, at 10 °C/min up to the flow temperature of each melt.

3. Results and discussion

3.1. Chemical composition

The chemical analyses (in mol%) by XRF and ICP-OES are presented in Table 1, the deviations (ND) and variations among the compositions (σ) are negligible.

3.2. Structural evaluation

The X-ray diffraction patterns of the Gx compositions are shown in Fig. 1. All glasses exhibit typical spectra for amorphous materials, with halos centered at approximately $2\theta = 22°$ and $2\theta = 33°$, which indicate the precursor short-range ordering of the atomic arrangements for the system's inherent crystalline phases, such as calcium and sodium silicate (Combeite High), if the structural equilibrium is favored, i.e., by thermal activation [28,29]. These results show that up to 8.0 mol% of Nb_2O_5 can be incorporated to this glass system without growth of crystalline phases, as expected.

For insight on the coordination of Nb atoms in the glass network structure, ^{93}Nb MAS-NMR analyses were performed, and the spectra for the G6 and G8 compositions are shown in Fig. 2, with $LiNbO_3$ crystal spectrum obtained with the same experimental conditions, for comparison. The scale of isotropic chemical shifts for different NbO_x polyhedra [30,31] is shown in Table 2. Comparing the spectra of G6 and G8 glasses with the $LiNbO_3$ crystal spectrum, it is observed that they exhibit a much wider bandwidth, ranging from −2500 ppm to 0 ppm, which is due to the high quadrupolar interactions of the ^{93}Nb nuclei in the glassy phase. The noise of the spectra is due to the low Nb content in the glasses [31], and that is why only G6 and G8 glasses are shown. For quantitative evaluation on the Nb coordination, further analyses must be assessed by ^{93}Nb MQMAS-NMR. Nevertheless, changes in the ^{93}Nb chemical shift reflect the gradual transformation of the NbO_6 octahedron edge bonds from cationic to anionic or vice versa [30,31]. The Nb (V) coordination in most crystals (i.e., $LiNbO_3$) is octahedral [31]. Due to the range of chemical shift presented by the G6 and G8 spectra, our results qualitatively indicate that niobium is present in the glasses in the NbO_6 octahedral coordination for all the Gx glasses, possibly coexisting with less coordinated NbO_x units in small sites of niobium-rich phases, indicated by the decrease in chemical shift with higher Nb content. These octahedra have a perovskite structure type, which is charge balanced by R^+ and R^{2+} ions [31].

The MAS-NMR spectra for the ^{29}Si nuclei are shown in Fig. 3-a, and provide qualitative information on the connectivity of the SiO_4 tetrahedra. Comparing the G0 glass spectrum with the spectra of glasses G2 – G8, asymmetric bands are observed for all compositions, corresponding

Table 1
Chemical composition (mol %) of the glasses by XRF and ICP-OES, medium deviation (%) from the nominal composition (ND) and variation (σ) of oxides among compositions.

Sample	SiO_2	B_2O_3	Na_2O	CaO	K_2O	Al_2O_3	Nb_2O_5
G0	44.0	7.4	22.8	19.8	0.7	5.2	0.0
G2	46.1	6.7	24.5	16.1	0.7	4.0	1.9
G4	42.2	7.2	23.0	17.3	0.6	6.3	3.5
G6	42.6	6.9	23.2	15.3	0.6	5.8	5.6
G8	39.5	7.0	22.2	16.7	0.7	6.1	7.8
ND	2.3	0.3	1.9	4.3	0.0	3.5	0.2
σ	2.7	0.3	0.8	1.7	0.0	0.9	2.5

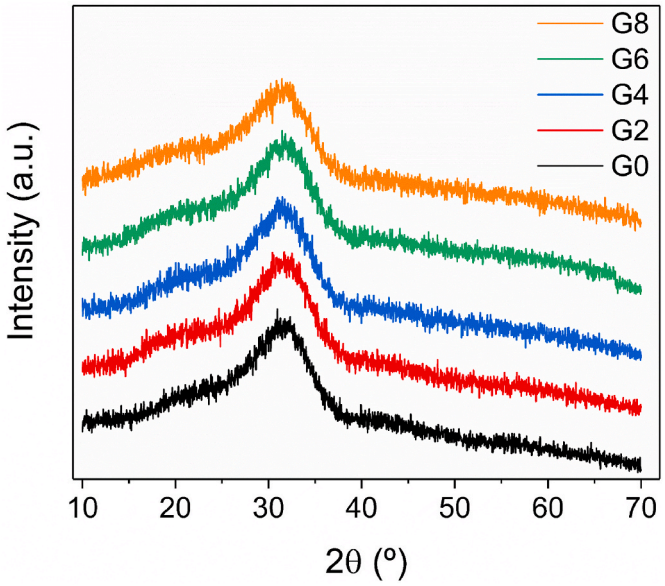

Fig. 1. X-ray diffraction patterns of the Gx compositions.

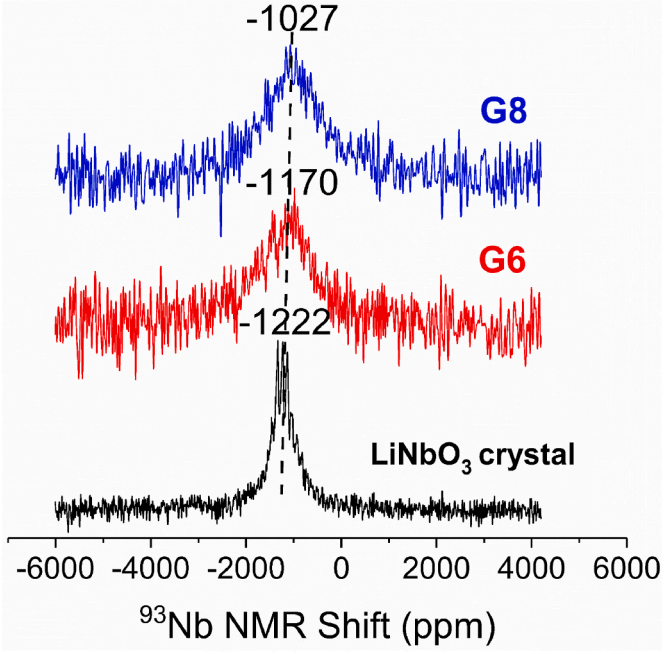

Fig. 2. ^{93}Nb MAS-RMN of G6 and G8 glasses.

Table 2
Isotropic chemical shifts related to different coordination of Nb sites in niobate crystals and comparison to the ^{93}Nb MAS-NMR results.

Nb sites	Chemical shift (ppm)	Reference	Sample
Four-coordinated Nb sites (NbO_4)	−650 to −950	30, 31	
Five-coordinated Nb sites (NbO_5)	−920 to −1000	30, 31	
Six-coordinated Nb sites (NbO_6)	−900 to −1300	30, 31	G6 and G8

mostly to Q^2 units, (around −82 ppm), coexisting with Q^3 units (around −90 ppm) and Q^1 (around −75 ppm) [32,33]. All spectra are centered at ≈ −82 ppm, but the different niobia contents in G2, G4 and G6 spectra do not clearly present changes in ppm, except for G8 which is slightly shifted to lower ppm, indicating higher concentration of Q^1 units for this composition. Due to the very low Nb–Si solubility [34], the Nb^{5+} ions do not tend to act as glass formers in silicate glasses, but rather interact with non-bridging oxygens (NBO) of SiO_4 tetrahedra, and cations such as Na^+, K^+ and Ca^{2+} for charge balance. Contributions of the band around −103 ppm, related to Q^4 units [35], are not observed in the spectrum of any composition, indicating a high degree of depolymerization. The ^{29}Si MAS-NMR data presented in Fig. 3-a gives insight of the silicate network as mostly constituted of two-dimensional chain structures, in overlapping planes of connected SiO_4 tetrahedra [36–39].

The ^{11}B MAS-NMR results are shown in Fig. 3-b, where the spectra are scaled on the BO_4 peak to the same height (normalized). The spectra of all compositions reveal that boron participates in the glass structure in both trigonal BO_3 and tetragonal BO_4 coordination, which is usual for this family of glasses because of phase-to-phase separations involving silica-rich and boron-rich phases [40–42]. However, it is clear that by adding niobia to the glasses, the ratio BO_3/BO_4 changes, indicating an increase in BO_3 species for G4, G6 and G8. The G2 glass exhibits the lowest BO_3 fraction, and this might be due to its slightly higher content of SiO_2 (see Table 1), when compared to the other compositions. With more SiO_4 tetrahedra to be charge balanced, boron promptly stabilizes the glass network structure by acting as a glass former (BO_4) [40–42]. For the case of the BO_4 peak, differences in chemical shift have been attributed to changes in BO_4 structural units in function of the B_2O_3 content [41,42]. Also, the peak gradually shifts to higher frequencies as the number of surrounding Si atoms decrease, and vice-versa. In the Gx glasses, the B_2O_3 content is rather stable among all compositions, and this suggests that the number of Si atoms surrounding BO_4 units tends to decrease with the additions of niobia, due to the conversion of BO_4 to BO_3, for G4, G6 and G8 glasses. For a quantitative analysis of the BO_3/BO_4 ratio by deconvolution and fitting of the respective bands using appropriate quadrupolar constants, future ^{11}B MQMAS-NMR is necessary. Burnett et al. [43] when studying the Na_2O–Nb_2O_5–B_2O_3 system, observed that low Nb_2O_5 contents are enough to create an immiscibility gap, where high binding energy cations can compete with B for their coordination with oxygen. In the case of Nb^{5+} ions, the stabilization in the symmetrical structure of perovskite is a determining factor in favoring the reduction of its free energy. Also, there is a competition between boron and niobium in balancing residual charges in this system with Na^+ ions, as the number of oxygens in NbO_6 octahedra is higher than in BO_3 and BO_4 units. Moreover, the incompatibility between the perovskite structure and the planar ring and non-ring boron structures is well known [44,45]. Therefore, even though NbO_6 octahedra might also be charge balanced by Ca^{2+} and K^+ ions, present in the Gx glasses, these results strongly indicate that, in this complex system, NbO_6 octahedra are preferentially being charge balanced by Na^+ ions. This explains the boron speciation in Gx glasses, once they depend on the local availability of Na^+. For the case of possible NbO_4 units, they constitute the niobium-rich phase [31,44,45], so they do not interfere in the borate units.

The aluminum coordination in these glasses has already been evaluated [10] and is tetrahedral, especially due to the fact that Al/Si ratio is very low in all Gx glasses, which favors the Al-avoidance, that is, T-O-T linkages (T = Al and Si) in the place of Al–O–Al, and aluminum is four-coordinated to act as a glass former. Literature data [37–42] report that in soda-lime silicate and borosilicate glasses, the Na^+ and Ca^{2+} surrounding network is similar, that is, Ca^{2+} can easily replace Na^+, as the number of first neighbors (coordination) is around 6 for Ca^{2+} and 5

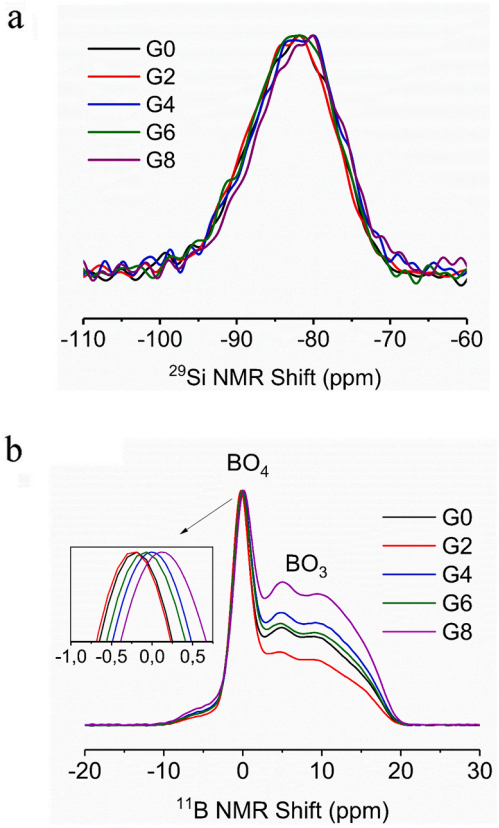

Fig. 3. (a) ^{29}Si MAS-NMR and (b) ^{11}B MAS-NMR normalized (0,1) spectra obtained from the Gx glass compositions.

for Na^+. Also, the molar ratios $Na_2O > Al_2O_3$, $Na_2O > B_2O_3$ and $Na_2O > Nb_2O_5$ suggest there is enough Na^+ ions for charge compensation of these structural units in the Gx glasses [33,38].

Complementing the studies performed by MAS-NMR, the Raman spectra obtained from the samples of Gx compositions are shown in Fig. 4. The band attributions of each structural unit are described in Table 3, and the relative area (%) of each deconvoluted band is shown in Table 4. For the Levenberg/Marquardt fitting method, all spectra presented a residuals standard deviation (σ) = 0.075 and R^2 = 0.996. It is known from the literature [26,27] that Si–O–Si and Al–O–Al linkages have very close stretching modes, and that T-O-T linkages modes are near 500 cm^{-1} and 560 cm^{-1}. However, the best fitting of our Raman data was achieved based on the model proposed by Manara et al. [26] and Lönartz et al. [27], considering 498 cm^{-1} for Si–O–Si and 560 cm^{-1} for T-O-T linkages.

Analyzing the spectra shown in Fig. 4 and comparing with the relative area (Table 4), it is possible observe that the presence of niobia in the glass structure cause the rupture of the silicate matrix, as indicated by the substantial area decrease of the band related to Si–O stretching in SiO_4 tetrahedra (498 cm^{-1}). The band at 560 cm^{-1} exhibits area decrease from G0-G8 glass, indicating the reduction in T-O-T stretching modes, also consistent with the changes in the number of BO's (bridging-oxygens). The band related to Danburite rings (Si–O–B–O–Si) exhibits an area increase only for G2 glass, being consistent with the ratio $BO_4 > BO_3$ for this composition, as boron acts as glass former through these structural rings in borosilicate glasses with high modifier concentrations (Na^+, Ca^{2+}) [33]. Changes in the bands BO_4 I (674 cm^{-1}) and BO_4 II (736 cm^{-1}), show the interference of niobia in these structures, leading to the existence of diborate groups at the expense of tetraborate ones. The emergence and area growth of the band at 816 cm^{-1} is due to the stretching of Nb–O–Nb bonds of highly distorted NbO_6 octahedra in the glass structure [11–13,18,45]. Besides that, the band shift from 814 cm^{-1} (G2) to 819 cm^{-1} (G8) indicates the increase in connectivity of these NbO_x polyhedra and less distortion [45]. This shift occurs due to the decreased octahedron coordination and Nb–O bond distance, resulting in increased vibration frequencies [31,45], as pointed by the trend in chemical shift observed in the ^{93}Nb MAS-NMR (Fig. 2). The area changes in Table 4 show the rupture of Q^2 units and the rise of (Si–O–Si): R^+ stretching modes, as more niobia is added to the glasses. These alterations are attributed to the rupture of network structure, indicating that the Nb^{5+} ions also interact with R^+ cations associated to the SiO_4 tetrahedra for charge balance. The decrease of Q^2 units occurs simultaneously with changes in the concentration of Q^1 and Q^3 species, which is due to the good adaptability of the open network structure and to the boron speciation. In the boron-rich phase, the BO_3 I and BO_3 II bands (1295 and 1398 cm^{-1}) exhibit changes that are due to the growth of NBO's in the BO_3 units.

In Fig. 5, an illustrative scheme of the interaction of niobia with the Q^2 (the most predominant silicate matrix) is shown. Niobia incorporates in the silicate matrix by interacting with silicate NBO's and alkali ions such as Na^+, breaking Q^2 units to become Q^1, and inducing BO_4 units to become BO_3. Further Nb EXAFS experiments are necessary to testify this in this system. However, Piilonen et al. [46] observed, through combined XANES and EXAFS studies, that in Nb^{5+} environment in dry and fluid-rich (H_2O, F) peraluminous and peralkaline silicate glasses, these units share corners with SiO_4 and Al_2O_3 tetrahedra via non-bridging oxygen atoms (NBO's), which supports our results. The strong Nb–O–Nb bonds and the short-range order of the perovskite structure promptly needs charge stabilization for the oxygens occupying the corner and edges sites of the NbO_6 octahedra [31].

3.3. Thermal behavior

The differential thermal analysis (DTA) curves for G0, G2, G4, G6 and G8 glasses are shown in Fig. 6 and the determined temperatures are shown in Table 5. The curves exhibit mainly the glass transition interval T_g (around 490 °C), the temperature range where the samples start to crystallize T_{ic} due to the heating, and the temperature where the samples show the maximum crystallization T_c. It can be observed (Fig. 6) that the T_{ic} and T_c events changed to higher temperatures as more niobia was added for glasses G4, G6 and G8 (see Table 5), which is due to the increase of thermal resistance of these glasses. The glass transition Tg does not change with the growing concentration of niobia, suggesting that such low contents did not interfere in this temperature interval. An endothermic peak around 760 °C is observed in the DTA curves of G0, G4 and G8 glasses (Fig. 6), indicating the melting of crystals formed during the heating of these samples. The glasses G2 and G6 do not exhibit this peak, which in comparison to the other compositions, is probably due to differences in connectivity of the network structure involving NBO's, where higher displacement of atoms facilitate the melting of crystals [3,4,13].

The stability, i.e., resistance to crystallization was assessed through the Hruby parameter (K_H) [47], and the determined values are shown in Table 5. An increase in K_H can be observed as more niobia is added to the glasses from G2 to G8, showing that the oxide, in controlled composition (low contents), is a potential candidate for use in conditions where the growth of heat-induced crystalline phases in the matrix should be avoided or minimized. The processing window ΔT (T_{ic}-T_g) exhibit a trend of increase from G2 – G6, in accordance with K_H value for these

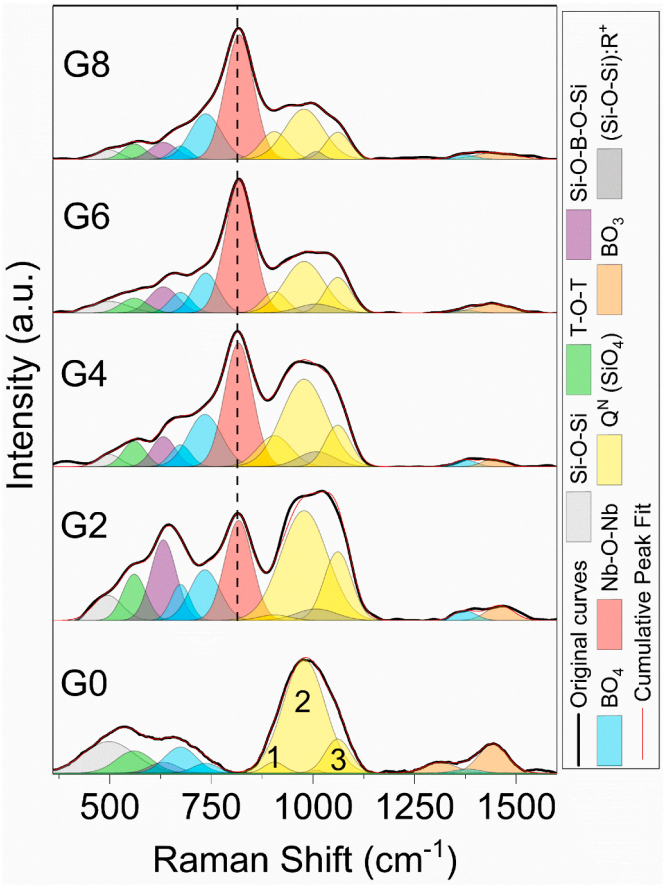

Fig. 4. Room temperature Raman spectra obtained from the Gx glass compositions.

Table 3
Raman bands related to the selected structural units present in the Gx glasses.

Attribution	Raman Shift (cm^{-1})	Reference
Si–O–Si stretching mode	498	26,27
T-O-T stretching (T = Si, Al)	560	26,27
Si–O–B–O–Si Borosilicate unit	632	26,27
BO_4 Tetraborate groups	674	26,27
BO_4 Diborate groups	736	26,27
Nb–O–Nb short stretching in NbO_6 units	~816	45,48
Q_1 units of SiO_4 tetrahedron	905	26,27
Q_2 units of SiO_4 tetrahedron	978	26,27
$(Si–O–Si):R^+$	1008	27
Q_3 units of SiO_4 tetrahedron	1061	26,27
Q_4 units of SiO_4 tetrahedron	1129	26,27
BO_3-BO_4 stretching in boron-rich phase	1295,1450,1398	26,27

compositions containing up to 6.0 mol% of Nb_2O_5. These results show that niobia helps to increase the resistance of these glasses to crystallize up to 6 mol% (G6), due to the cross-linking character and refractoriness of the NbO_6 octahedra. The decrease of Tc and ΔT for G8 glass might be due to the growth of niobium-rich phases [48].

The viscosity points determined in the hot-stage microscopy (HSM) analyzes were plotted in function of the heating temperature (±5 °C), and are shown in Fig. 7. Analyzing the plotted data, it was confirmed that the compositions G0 and G2 resist to elevated temperatures (≈850 °C) and then flow almost catastrophically, with little variation in temperature. The G4, G6 and G8 glasses, on the other hand, exhibit relaxation with a gradual increase until reaching the state of total fluency at the temperatures expected for the parent glass composition (G0). There are, therefore, two distinct types of flow behavior: G0 and G2 are strong glasses (highly viscous) and G4, G6 and G8 are weak glasses (less viscous). We observed a close relation of the viscosities with the ^{11}B MAS-NMR results (Fig. 3-b), as G4, G6 and G8 glasses (less viscous) exhibited more BO_3 fraction, so we relate the changes in viscosities to the boron speciation in the glasses, once a decrease in BO_4 units (glass formers) strongly influence the viscosities of these glasses [8,33,41].

Table 4
Relative area (%) of deconvoluted Raman bands (σ = 0.075; R^2 = 0.996).

Raman Band	Relative area (%)				
Sample	G0	G2	G4	G6	G8
Si–O–Si	14.76	4.26	2.02	4.10	2.28
T-O-T	7.25	6.34	4.06	3.67	3.51
Si–O–B–O–Si	2.78	11.94	5.01	6.77	4.50
BO_4 I	7.58	4.05	3.17	4.10	2.50
BO_4 II	2.23	8.94	12.44	9.24	14.10
Nb–O–Nb	0	16.09	24.64	33.68	35.10
Q^1	2.04	1.04	7.34	4.72	7.50
Q^2	43.63	29.87	27.73	18.58	19.18
$(Si–O–Si):R^+$	0.26	2.76	3.82	3.07	1.10
Q^3	7.80	11.01	7.47	8.33	6.51
BO_3 I	3.11	0	0	0	0
BO_4 III	0.93	1.32	1.11	0.61	0.99
BO_3 II	7.63	2.38	1.19	3.13	2.73
Total area (%)	100	100	100	100	100

The addition of up to 8 mol% of niobia to the Gx glasses has then proven to indirectly contribute to the decrease in the viscosity of their melts, through boron speciation. Therefore, the use of niobia in controlled dispersity is an alternative for lowering the viscosity of silicate melts without substantial changes in the glass matrix Q^n configuration. These characteristics stand out as a new family of niobium-modified borosilicate glasses to be used in applications where self-heating processes take place, such as nuclear waste immobilization, due to radiation-induced heating [49].

4. Conclusions

The structural and thermal interference of niobia in aluminoborosilicate glasses were evaluated after low additions up to 8.0 mol% of Nb_2O_5, promoting only a distortion in the network structure and avoiding the significant growth of niobium-rich phases. For this compositional range, the oxide incorporated into the network structure as a modifier agent (NbO_6 octahedra). As a result, it ruptured part of the silicate matrix and interfered in the boron speciation, but the predominance of the Q^2 species was maintained, preserving the ability of element incorporation of these compositions. Thermally, the oxide contributed to the increase in resistance to crystallization (K_H) and processing window (G2-G6) of the glasses due to the cross-linking of the NbO_6 octahedra. The niobia additions also impacted in the shrinkage and flow behavior of the glasses, with a notable decrease in the viscosity of the melts, due to the boron speciation in response to the niobia additions. This new family of niobium-modified borosilicate glasses is a promising material for the treatment of hazardous wastes, potentially encouraging the green energy production.

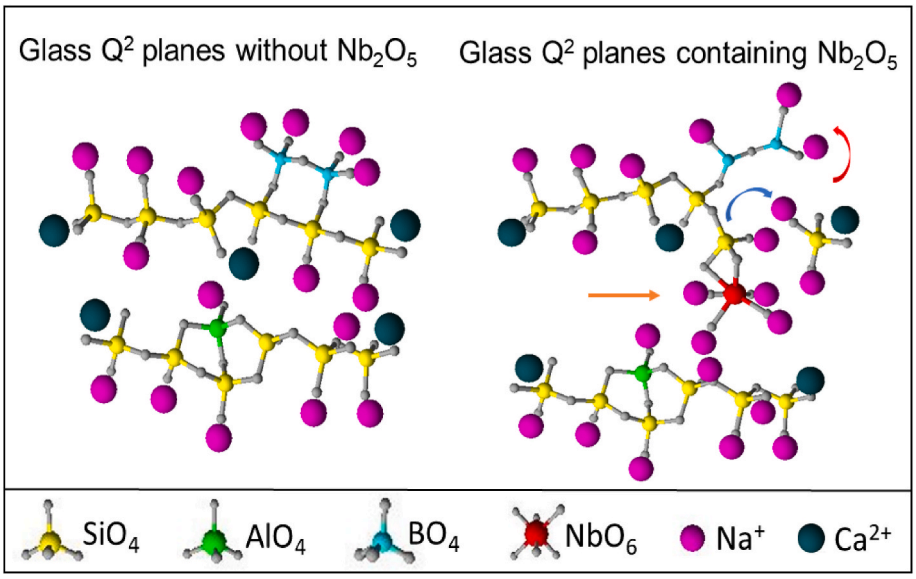

Fig. 5. Illustrative scheme of Q^2 planes in the silicate structure, showing the rupture of Q^2 network structure by NbO_6 octahedra, resulting in Q^1 and BO_3 units.

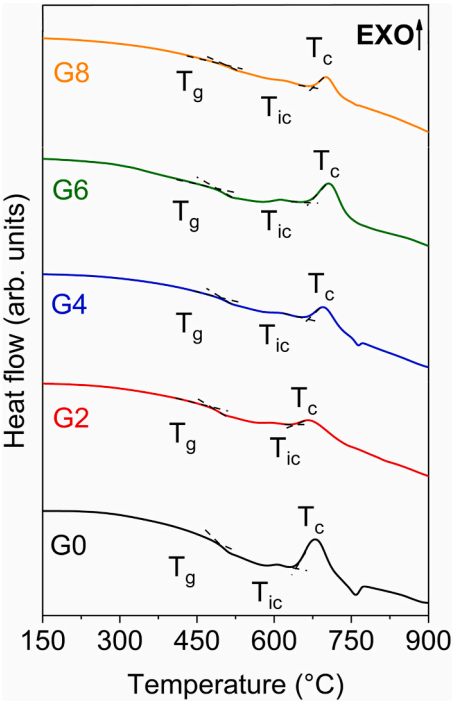

Fig. 6. DTA curves obtained for the glass samples of compositions G0, G2, G4, G6, and G8 showing the T_g (glass transition), T_{ic} (initial crystallization) and T_c (maximum crystallization).

Table 5
Temperatures (°C) of glass transition (T_g), initial crystallization (T_{ic}), maximum crystallization (T_c), stability parameter (K_H) and processing window (ΔT), determined from the DTA curves.

Sample	G0	G2	G4	G6	G8
T_g (±2 °C)	485 °C	474 °C	487 °C	485 °C	486 °C
T_{ic}(±2 °C)	640 °C	637 °C	662 °C	670 °C	673 °C
T_c(±2 °C)	678 °C	667 °C	695 °C	706 °C	700 °C
ΔT (±2 °C)	155	163	175	185	169
K_H	0.4	0.5	0.6	0.6	0.6

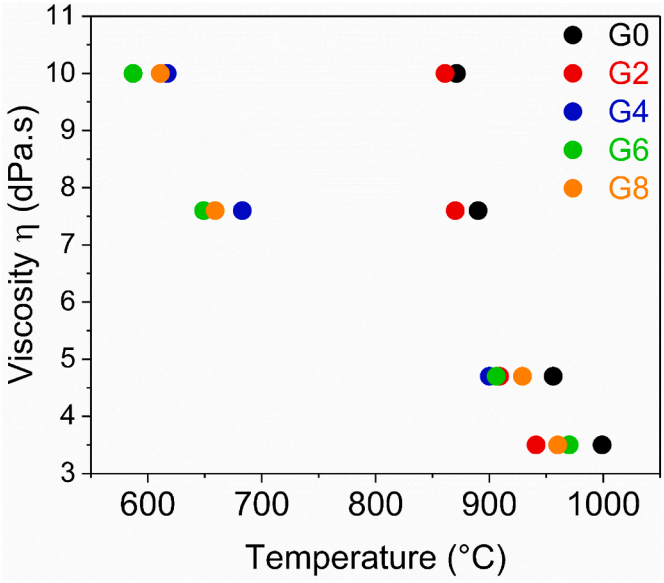

Fig. 7. Viscosities of the Gx glasses as a function of the heating temperature during the HSM tests.

Declaration of competing interest

The authors declare that they have no known competing financial interests or personal relationships that could have appeared to influence the work reported in this paper.

Acknowledgements

This work was supported by the Coordination of Superior Level Staff Improvement (CAPES) with the CAPES-Eletronuclear project n°81/2013, by the São Paulo Research Foundation (FAPESP) Projects n.1999/01924-2 and n.2000/02483-9, and by the National Council for Scientific and Technological Development (CNPq), Projects n.481260/2012 and n.312135/2016-5. The authors thank Igor Yamamoto Abe, from the Electrical Engineering Department of the Polytechnic School of the University of São Paulo (USP) for the Raman spectroscopy measurements, and Isabel Sobrados, from the Materials Science Institute of

Madrid-Spain (ICMM), for the MAS-NMR measurements.

References

[1] X. Lu, L. Deng, J. Du, J.D. Vienna, Predicting boron coordination in multicomponent borate and borosilicate glasses using analytical models and machine learning, J. Non-Cryst. Sol. 553 (2021) 120490, https://doi.org/10.1016/j.jnoncrysol.2020.120490.

[2] Z.A. Alrowaili, A.M. Al-Baradi, M.A. Sayed, A.M. Ali, E.A. Wahab, M.S. Al-Buriahi, K.S. Shaaban, The impact of Fe_2O_3 on the dispersion parameters and gamma/fast neutron shielding characteristics of lithium borosilicate glasses, Optik 249 (2022) 168259, https://doi.org/10.1016/j.ijleo.2021.168259.

[3] R. Bouakkaz, A. Abdelouas, B. Grambow, Kinetic study and structural evolution of SON68 nuclear waste glass altered from 35 to 125° C under unsaturated H_2O and D_2O_{18} vapour conditions, Corrosion Sci. 134 (2018) 1–16, https://doi.org/10.1016/j.corsci.2017.12.035.

[4] D.L. McClane, K.M. Fox, F.C. Johnson, J.W. Amoroso, A.A. Kruger, Dissolution of accumulated spinel crystals in simulated nuclear waste glass melts, J. Hazar. Tox. Radioac. Wst. 22 (2018), 05018001, https://doi.org/10.1061/(ASCE)HZ.2153-5515.0000388.

[5] S.A. Luksic, D.S. Kim, W. Um, G. Wang, M.J. Schweiger, C.Z. Soderquist, A. A. Kruger, Effect of Technetium-99 sources on its retention in low activity waste glass, J. Nucl. Mater. 503 (2018) 235–244, https://doi.org/10.1016/j.jnucmat.2018.02.019.

[6] J.C. Lee, B.K. Jang, C.S. Shon, J.H. Kim, C.W. Chung, Potential use of borosilicate glass to make neutron shielding mortar: enhancement of thermal neutron shielding and strength development and mitigation of alkali-silica reaction, J. Clean. Prod. 210 (2019) 638–645, https://doi.org/10.1016/j.jclepro.2018.11.033.

[7] A.C. Silva, S.M. Castanho, Silicate glasses obtained from fine silica powder modified with galvanic waste addition, J. Non-Cryst. Sol. 348 (2004) 211–217, https://doi.org/10.1016/j.jnoncrysol.2004.08.171.

[8] A.C. Silva, S. Mello- Castanho, F. Guitian, I. Montero, A. Esteban- Cubillo, I. Sobrados, J.S. Moya, Incorporation of galvanic waste (Cr, Ni, Cu, Zn, Pb) in a soda–lime–borosilicate glass, J. Am. Ceram. Soc. 91 (2008) 1300–1305, https://doi.org/10.1111/j.1551-2916.2008.02311.x.

[9] A.C. Silva, S.C. Santos, S.R.H. Mello-Castanho, Transition metals in glass formation, Mater. Sci. Found. 727 (2012) 1496–1501. http://dx.doi.org/10.4028/www.scientific.net/MSF.727-728.1496.

[10] J.S. Moya, B. Cabal, J. Sanz, A.C. Da Silva, S. Mello-Castanho, R. Torrecillas, R. Rojo, Mechanism of calcium lixiviation in soda-lime glasses with a strong biocide activity, Mater. Lett. 70 (2012) 113–115, https://doi.org/10.1016/j.matlet.2011.11.104.

[11] F.F. Sene, J.R. Martinelli, L. Gomes, Synthesis and characterization of niobium phosphate glasses containing barium and potassium, J. Non-Cryst. Sol. 348 (2004) 30–37, https://doi.org/10.1016/j.jnoncrysol.2004.08.122.

[12] H. Maeda, S. Lee, T. Miyajima, A. Obata, K. Ueda, T. Narushima, T. Kasuga, Structure and physicochemical properties of $CaO–P_2O_5–Nb_2O_5–Na_2O$ glasses, J. Non-Cryst. Sol. 432 (2016) 60–64, https://doi.org/10.1016/j.jnoncrysol.2015.06.003.

[13] I.L. Denry, J.A. Holloway, R.J. Nakkula, J.D. Walters, Effect of niobium content on the microstructure and thermal properties of fluorapatite glassceramics, J. Biomed. Mater. Res. Part B: Appl. Biomat. 75 (2005) 18–24, https://doi.org/10.1002/jbm.b.30295.

[14] L.P. de Souza, J.H. Lopes, F.V. Ferreira, R.A. Martin, C.A. Bertran, J.A. Camilli, Evaluation of effectiveness of 45S5 bioglass doped with niobium for repairing critical- sized bone defect in in vitro and in vivo models, J. Biomed. Mater. Res. Part A. 108 (2020) 446–457, https://doi.org/10.1002/jbm.a.36826.

[15] V. Miguez-Pacheco, D. De Ligny, J. Schmidt, R. Detsch, A.R. Boccaccini, Development and characterization of niobium-releasing silicate bioactive glasses for tissue engineering applications, J. Eur. Ceram. Soc. 38 (2018) 871–876, https://doi.org/10.1016/j.jeurceramsoc.2017.07.028.

[16] G. de Souza Balbinot, F.M. Collares, T.L. Herpich, F. Visioli, S.M.W. Samuel, V.C. B. Leitune, Niobium containing bioactive glasses as remineralizing filler for adhesive resins, Dent. Mater. 36 (2020) 221–228, https://doi.org/10.1016/j.dental.2019.11.014.

[17] B. Samuneva, V. Dimitrov, Structure and optical properties of niobium silicate glasses, J. Non-Cryst. Sol. 129 (1991) 54–63, https://doi.org/10.1016/0022-3093(91)90080-P.

[18] J.H. Lopes, A. Magalhães, I.O. Mazali, C.A. Bertran, Effect of niobium oxide on the structure and properties of melt-derived bioactive glasses, J. Am. Ceram. Soc. 97 (2014) 3843–3852, https://doi.org/10.1111/jace.13222.

[19] M.S.P. Francisco, Y. Gushikem, Synthesis and characterization of $SiO_2–Nb_2O_5$ systems prepared by the sol–gel method: structural stability studies, J. Mater. Chem. 12 (2002) 2552–2558, https://doi.org/10.1039/B200685E.

[20] H.K. Dan, N.D. Trung, T.H. Le, N. Le Thai, N.M. Ty, D. Zhou, J. Qiu, Influence of F^- on the reduction process of Eu^{3+} to Eu^{2+} and optical properties of $Eu^{3+}/Eu^{2+}–Er^{3+}–Yb^{3+}$ co-doped niobate silicate glasses, J. Non-Cryst. Sol. 581 (2022) 121417, https://doi.org/10.1016/j.jnoncrysol.2022.121417.

[21] N.A. Wójcik, S. Ali, E.I. Kamitsos, D. Möncke, Niobate in silicate and phosphate glasses: effect of glass basicity on crucible dissolution, Int. J. Appl. Glass Sci. 13 (2022) 121–134, https://doi.org/10.1111/ijag.16505.

[22] E. Koroleva, A. Lipovskii, S. Petrunenkova, D. Tagantsev, S. Vakhrushev, In-situ study of the formation of sodium-niobate-silicate glass-ceramics with dielectric spectroscopy, J. Non-Cryst. Sol. 556 (2021) 120553, https://doi.org/10.1016/j.jnoncrysol.2020.120553.

[23] J. Wang, H. Song, X. Kong, H. Peng, B. Sun, B. Chen, H. Xia, Fluorescence properties of trivalent europium doped in various niobate co-doped glasses, J. Appl. Phys. 93 (2003) 1482–1486, https://doi.org/10.1063/1.1536726.

[24] M.P.F. Graça, M.A. Valente, M.F. da Silva, Electrical properties of lithium niobium silicate glasses, J. Non-Cryst. Sol. 325 (2003) 267–274, https://doi.org/10.1016/S0022-3093(03)00314-4.

[25] N.A. Wójcik, S. Ali, A. Mielewczyk-Gryń, B. Jonson, Two-step synthesis of niobium doped Na–Ca–(Mg)–P–Si–O glasses, J. Mater. Sci. 56 (2021) 7615–7625, https://doi.org/10.1007/s10853-021-05781-w.

[26] D. Manara, A. Grandjean, D.R. Neuville, Advances in understanding the structure of borosilicate glasses: a Raman spectroscopy study, Am. Mineral. 94 (2009) 777–784, https://doi.org/10.2138/am.2009.3027.

[27] M.I. Lönartz, L. Dohmen, C. Lenting, C. Trautmann, M. Lang, T. Geisler, The effect of heavy ion irradiation on the forward dissolution rate of borosilicate glasses studied in situ and real time by fluid-cell Raman spectroscopy, Mat 12 (2019) 1480, https://doi.org/10.3390/ma12091480.

[28] H.A. Abo-Mosallam, H. Darwish, S.M. Salman, Crystallization characteristic and properties of some zinc containing soda lime silicate glasses, J. Mater. Sci. Mater. Electron. 21 (2010) 889–896, https://doi.org/10.1007/s10854-009-0012-3.

[29] X. Chatzistavrou, N. Kantiranis, E. Kontonasaki, K. Chrissafis, L. Papadopoulou, P. Koidis, K.M. Paraskevopoulos, Thermal analysis and in vitro bioactivity of bioactive glass–alumina composites, Mater. Char. 62 (2011) 118–129, https://doi.org/10.1016/j.matchar.2010.11.008.

[30] O.B. Lapina, D.F. Khabibulin, K.V. Romanenko, Z. Gan, M.G. Zuev, V. N. Krasil'nikov, V.E. Fedorov, ^{93}Nb NMR chemical shift scale for niobia systems, Solid State Nucl. Magn. Reson. 28 (2005) 204–224, https://doi.org/10.1016/j.ssnmr.2005.09.003.

[31] A. Flambard, J.J. Videau, L. Delevoye, T. Cardinal, C. Labrugère, C.A. Rivero, L. Montagne, Structure and nonlinear optical properties of sodium– niobium phosphate glasses, J. Non-Cryst. Sol. 354 (2008) 3540–3547, https://doi.org/10.1016/j.jnoncrysol.2008.03.017.

[32] A.R. Jones, R. Winter, G.N. Greaves, I.H. Smith, MAS NMR study of sodalime–silicate glasses with variable degree of polymerization, J. Non-Cryst. Sol. 293 (2001) 87–92, https://doi.org/10.1016/S0022-3093(01)00656-1.

[33] H. Bradtmüller, T. Uesbeck, H. Eckert, T. Murata, S. Nakane, H. Yamazaki, Structural origins of crack resistance on magnesium aluminoborosilicate glasses studied by solid-state NMR, J. Phys. Chem. C 123 (2019) 14941–14954, https://doi.org/10.1021/acs.jpcc.9b03600.

[34] M. Ibrahim, N.F. Bright, The binary system Nb_2O_5—SiO_2, J. Am. Ceram. Soc 45 (1962) 221–222, https://doi.org/10.1111/j.1151- 2916.1962.tb11130.x.

[35] T. Ohkubo, R. Monden, Y. Iwadate, S. Kohara, K. Deguchi, S. Ohki, T. Shimizu, Structural investigation of aluminoborosilicate glasses containing Na_2MoO_4 crystallites by solid state NMR, Phys. Chem. Gl. – Eur. J. Gl. Sci. Tech. B (2015) 139–144, https://doi.org/10.13036/17533562.56.4.139.

[36] C. Le Losq, D.R. Neuville, W. Chen, P. Florian, D. Massiot, Z. Zhou, G.N. Greaves, Percolation channels: a universal idea to describe the atomic structure and dynamics of glasses and melts, Sci. Rep. 7 (2017) 1–12, https://doi.org/10.1038/s41598-017-16741-3.

[37] S.K. Lee, J.F. Stebbins, The distribution of sodium ions in aluminosilicate glasses: a high-field Na-23 MAS and 3Q MAS NMR study, Geochem, Cosmochem. Act. 67 (2003) 1699–1709, https://doi.org/10.1016/S0016- 7037(03)00026-7.

[38] L. Cormier, G. Calas, B. Beuneu, Structural changes between soda-lime silicate glass and melt, J. Non-Cryst. Sol. 357 (2011) 926–931, https://doi.org/10.1016/j.jnoncrysol.2010. 10. 014.

[39] K. Januchta, R.E. Youngman, A. Goel, M. Bauchy, S.J. Rzoska, M. Bockowski, M. M. Smedskjaer, Structural origin of high crack resistance in sodium aluminoborate glasses, J. Non-Cryst. Sol. 460 (2017) 54–65, https://doi.org/10.1016/j.jnoncrysol.2017.01.019.

[40] F. Angeli, T. Charpentier, P. Jollivet, D. de Ligny, M. Bergler, A. Veber, H. Li, Effect of thermally induced structural disorder on the chemical durability of International Simple Glass, npj Mat. Degrad. 2 (2018) 1–11, https://doi.org/10.1038/s41529-018-0052-3.

[41] F. Angeli, O. Villain, S. Schuller, T. Charpentier, D. de Ligny, L. Bressel, L. Wondraczek, Effect of temperature and thermal history on borosilicate glass structure, Phys. Rev. B 85 (2012), https://doi.org/10.1103/PhysRevB.85.054110, 054110-054111 - 054110-14.

[42] N. Stone-Weiss, E.M. Pierce, R.E. Youngman, O. Gulbiten, N.J. Smith, J. Du, A. Goel, Understanding the structural drivers governing glass–water interactions in

borosilicate-based model bioactive glasses, Acta Biomater. 65 (2018) 436–449, https://doi.org/10.1016/j.actbio.2017.11.006.

[43] D. Burnett, D. Clinton, R.P. Miller, Some phase relationships within the system $Na_2O/B_2O_3/Nb_2O_5$, J. Mater. Sci. 3 (1968) 47–60, https://doi.org/10.1007/BF00550889.

[44] A.P. Malakho, S.Y. Stefanovich, V.A. Morozov, B.I. Lazoryak, E. Fargin, V. Rodriguez, Crystallization and dielectric and optical properties of borate glasses $(1-x)\ Na_2B4O_7+xNb_2O_5$, Russ. J. Inorg. Chem. 52 (2007) 301–307, https://doi.org/10.1134/S0036023607030011.

[45] G. Upender, M. Prasad, Raman, FTIR, thermal and optical properties of TeO_2-Nb_2O_5-B_2O_3-V_2O_5 quaternary glass system, J. Tai. Uni. Sci. 11 (2017) 583–592, https://doi.org/10.1016/j.jtusci.2016.02.008.

[46] P.C. Piilonen, F. Farges, R.L. Linnen, G.E. Brown Jr., M. Pawlak, A. Pratt, Structural environment of Nb^{5+} in dry and fluid-rich (H_2O, F) silicate glasses: a combined XANES and EXAFS study, Can. Mineral. 44 (2006) 775–794, https://doi.org/10.2113/gscanmin.44.3.775.

[47] A.F. Kozmidis-Petrović, Theoretical analysis of relative changes of the Hruby, Weinberg, and Lu–Liu glass stability parameters with application on some oxide and chalcogenide glasses, Thermochim. Acta 499 (2010) 54–60, https://doi.org/10.1016/j.tca.2009.10.023.

[48] H. Zheng, Y. Pu, X. Liu, J. Wan, Correlation between dielectric properties and crystallization treatment in potassium sodium niobate glass-ceramics for energy storage application, J. All. Comp. 674 (2016) 272–276, https://doi.org/10.1016/j.jallcom.2016 .03.025.

[49] S. Peuget, J.N. Cachia, C. Jégou, X. Deschanels, D. Roudil, V. Broudic, J.M. Bart, Irradiation stability of R7T7-type borosilicate glass, J. Nucl. Mater. 354 (2006) 1–13, https://doi.org/10.1016/j.jnucmat.2006.01.021.